Spin-glass behavior in dilute magnetic alloys with hcp structure

P. Gash,* R. Roshko, and O. G. Symko
Department of Physics, University of Utah, Salt Lake City, Utah 84112
(Received 20 August 1981)

A simple physical model is presented for calculating the magnetization of dilute magnetic systems with hcp hosts which incorporates elements of both crystal-field theory and the molecular-field theory of spin-glasses. To permit the computation of the Ruderman-Kittel-Kasuya-Yosida contribution, the interaction between the impurities is described by a randomly oriented effective internal exchange field $\vec{h}$ with a probability distribution $P(\vec{h})=\Delta/\pi^2(\Delta^2+h^2)^2$, where Δ is the most probable value of the internal field. The observed crystal-field effects are analyzed in terms of an ionic fine-structure Hamiltonian of the form DS_Z^2, with the fine-structure parameter D proportional to spin-orbit coupling to second order. The model is used to account for the measured magnetization of both single-crystal *Mg*Mn and polycrystalline *Zn*Mn alloys.

I. INTRODUCTION

Recent low-temperature magnetization measurements[1-4] on very dilute (<100 ppm) magnetic systems such as *Mg*Mn, *Zn*Mn, and *Zn*Cr have shown that the crystalline electric field of the host can play a substantial role in determining the magnetic behavior of the impurity, in particular the nature of its ground state. In addition to such single-impurity effects, these measurements also reveal the presence of a concentration-dependent interaction which causes the low-temperature magnetization (per impurity) to decrease with increasing impurity concentration, and which is attributed to a Ruderman-Kittel-Kasuya-Yosida (RKKY)-type coupling between the magnetic impurities. In this paper, we present a simple physical model for dilute magnetic systems consisting of $3d$ transition impurities dissolved in hcp host metals which can account for the measured magnetization and which incorporates elements of both crystal-field theory and the molecular-field theory of spin-glasses.

There are currently two approaches with which to describe the behavior of magnetic impurities dissolved in metals: the ionic model (Hirst[5]) and the virtual bound-state model (Blandin and Friedel,[6] Anderson[7]). In the ionic approach, the impurity is assumed to possess a well-defined configuration d^n (or f^n) and the mixing interaction between the atomic d orbitals and the conduction-band states of the host is treated as a weak perturbation on the free-ion energy-level structure; on the other hand, in the virtual bound-state model of Anderson (within the Hartree-Fock approximation) the mixing interaction is assumed to dominate. However, in spite of these differences, both the ionic model and the virtual bound-state model predict that, when the orbital angular momentum of the impurity is quenched by crystal fields, there will be a fine-structure splitting of the impurity energy levels due to the combined effects of the crystal field and spin-orbit coupling which, in systems with axial symmetry, has the form[8,9] DS_Z^2 (with $D\alpha\lambda^2$, where λ is the spin-orbit coupling constant). Moreover, both models yield a long-range Heisenberg-like exchange coupling between the impurity spins (mediated by the conduction electrons) of the form $\sum_{i,j}J(R_{ij})\vec{S}_i\cdot\vec{S}_j$, where $J(R_{ij})$ is an oscillating function of the interimpurity separation R_{ij} with an asymptotic form for large impurity separations given by $A\cos(2k_FR_{ij}+\Phi)/(k_FR_{ij})^3$. In the virtual bound-state model this exchange interaction is referred to as double-resonance coupling[10] and $A=(25/2\pi)E_F\sin^2\theta$ and $\Phi=\Phi(\phi,E_F)$, where ϕ is a scattering phase shift. In the ionic model, the exchange coupling mechanism between the impurity spins is known as the RKKY interaction[11] and $\Phi=0$ and $A=9\pi Z^2J^2/8E_f$, where J is the s-d exchange integral between the localized d electrons and the conduction electrons and Z is the number of conduction electrons per host atom.

Whether approached from the point of view of the ionic model or the virtual bound-state model, the magnetic exchange interaction between the impurities can be described by an effective internal exchange field such that the effective field seen by the ith impurity due to all the other impurities is $\vec{h}_i=\sum_J J(R_{ij})\vec{S}_j$. The oscillatory nature of the in-

teraction coupled with the randomness in the positions of the impurities means that the effective field $\vec{h}_i$ is the random variable and hence can be described by a continuous probability distribution $P(\vec{h})$. This internal field distribution has been derived for both the one-dimensional Ising Hamiltonian[12] and the full three-dimensional Heisenberg Hamiltonian[13–15]; for the Heisenberg interaction it is given by $P(\vec{h})=\Delta/\pi^2(h^2+\Delta^2)^2$. This is the form of the distribution which is used in the present calculation since it has been shown, by Walker and Walstedt,[15] to bear a close resemblance to the distribution of internal fields obtained from computer simulations of a spin-glass. Moreover, the parameter Δ has a well-defined physical interpretation: It is the most probable value of the magnitude of the internal exchange field.

In Sec. II we present the Hamiltonian for the model hcp-host—$3d$-transition-impurity system and we develop expressions for the magnetization for both single-crystal and polycrystalline samples as a function of temperature. In Sec. III we discuss the numerical integration techniques required to evaluate the theoretical expressions for the magnetization, and in Sec. IV we compare the calculated magnetization with the measured magnetization of a 5 ppm single crystal of *Mg*Mn and several polycrystalline samples of *Zn*Mn of varying concentration.

II. THE MODEL

The model for our system consisting of a $3d$ transition impurity dissolved dilutely in an hcp host metal includes the effects of an external field $\vec{H}_0$, an internal exchange field $\vec{h}$, and the crystal field due to the host. Figure 1 shows the relative orientations of the internal field, the external field, and the symmetry axis (c axis) of the crystal at one impurity site with respect to a fixed laboratory coordinate system xyz. The Hamiltonian for this model has the following form:

$$\mathscr{H}=\mathscr{H}_{\rm cf}+\mathscr{H}_{\rm int}+\mathscr{H}_{\rm ext}\ . \tag{1}$$

The first term $\mathscr{H}_{\rm cf}$ represents the effect of the host's crystal field. If the orbital levels of the impurity are split by the crystal field in such a way that the orbital angular momentum in the lowest level (or group of levels) is quenched, then the spin-orbit coupling between the ground level and excited orbital levels, in combination with the crystal field, will produce a fine-structure splitting of the $(2S+1)$-degenerate spin multiplet which, up to second order in λ (the spin-orbit coupling constant), has the form[16] $\vec{S}\cdot\underline{D}\cdot\vec{S}$. In the principal axis system of the crystal, the $\underline{D}$ tensor is given by[17]

$$\underline{D}=\begin{bmatrix} -\frac{D}{3} & 0 & 0 \\ 0 & -\frac{D}{3} & 0 \\ 0 & 0 & \frac{2D}{3} \end{bmatrix}. \tag{2}$$

After transformating the $\underline{D}$ tensor from the principal axis system to the xyz coordinate system in Fig. 1, the crystal-field contribution $\vec{S}\cdot\underline{D}\cdot\vec{S}$, to the spin Hamiltonian, becomes

$$\begin{aligned}\mathscr{H}_{\rm cf}=&\,D(\cos^2\phi\sin^2\theta-\tfrac{1}{3})S_x^2+D(\sin^2\phi\sin^2\theta-\tfrac{1}{3})S_y^2+D(\cos^2\theta-\tfrac{1}{3})S_z^2\\&+D\sin\phi\cos\phi\sin^2\theta(S_xS_y+S_yS_x)+D\cos\phi\cos\theta\sin\theta(S_xS_z+S_zS_x)\\&+D\sin\phi\cos\theta\sin\theta(S_yS_z+S_zS_y)\ ,\end{aligned} \tag{3}$$

where S_x, S_y, and S_z are the appropriate $(2S+1)\times(2S+1)$ spin matrices and where θ and ϕ are the polar angles which specify the orientation of the c axis with respect to xyz.

The second term in the Hamiltonian $\mathscr{H}_{\rm int}$ describes the effect of the internal exchange field which arises from the exchange coupling between the impurity spins. At a given impurity site it has the form of a Zeeman interaction between the impurity spin $\vec{S}$ and the local internal field $\vec{h}$:

$$\begin{aligned}\mathscr{H}_{\rm int}=&\,g\mu_B\vec{S}\cdot\vec{h}\\=&\,g\mu_Bh(S_x\sin\theta'\cos\phi'+S_y\sin\theta'\sin\phi'\\&+S_z\cos\theta')\ ,\end{aligned} \tag{4}$$

where θ' and ϕ' define the orientation of $\vec{h}$ in the xyz coordinate system in Fig. 1, and μ_B is the Bohr magneton. As pointed out in the Introduction, the randomness in the positions of the impur-

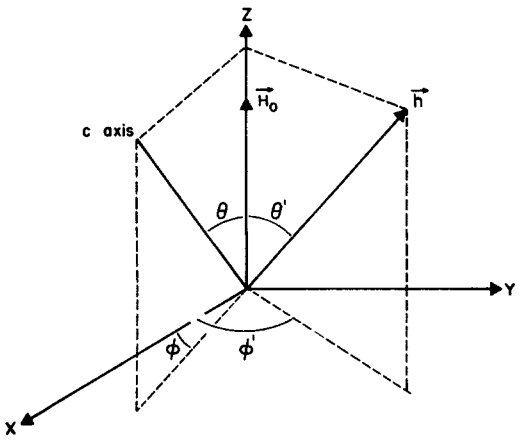

FIG. 1. Orientation of the external field $\vec{H}_0$ relative to the internal field $\vec{h}$ and the c axis of the crystal.

ities together with the oscillatory character of the exchange interaction ensure that the internal field $\vec{h}$ will be random variable which can be represented by a continuous probability distribution $P(\vec{h})$. For the three-dimensional Heisenberg form of the interaction, $\sum_{i,j} J_{ij}\vec{S}_i\cdot\vec{S}_j$, with $J_{ij}=A\cos(2k_F R_{ij})/(k_F R_{ij})^3$, the distribution is given by[13–15]

$$P(\vec{h})=\frac{\Delta}{\pi^2}\frac{1}{(\Delta^2+h^2)^2}\ . \tag{5}$$

The parameter Δ is the most probable value of the magnitude of the internal exchange field and is proportional to both the coefficient A in J_{ij} and to the impurity concentration.

The third term in the Hamiltonian $\mathscr{H}_{\rm ext}$ represents the Zeeman interaction between the impurity spin and the external field $\vec{H}_0$ and has the form

$$\mathscr{H}_{\rm ext}=g\mu_B\vec{S}\cdot\vec{H}_0\ . \tag{6}$$

If the eigenstates and eigenvalues of the Hamiltonian in Eq. (1) are known then the thermally averaged value of the component along the external field direction of the magnetic moment at the ith impurity site in a fixed internal field $\vec{h}_i$ can be obtained from the following expression:

$$\bar{\mu}_i(h_i,\theta_i',\phi_i',\theta,\phi)=\frac{\sum_n\langle n\,|\,g\mu_B S_z\,|\,n\rangle\exp(-E_n/k_BT)}{\sum_n\exp(-E_n/k_BT)}\ , \tag{7}$$

where the index n labels the various eigenstates $|\,n\,\rangle$ and the corresponding eigenvalues E_n, and θ and ϕ specify the orientation of the c axis with respect to the external field $\vec{H}_0$. The magnetization of the sample is obtained by summing the contributions $\bar{\mu}_i$ from all the impurities in the crystal or, equivalently, by averaging the quantity $\bar{\mu}$ for a single spin over all the possible values of the internal field using the probability distributions given in Eq. (5). For a single crystal with fixed values for θ and ϕ, the magnetization along the external field direction is given by

$$M_{\rm sing}=NC\int\bar{\mu}(\vec{h},\theta,\phi)P(\vec{h})d\vec{h}\ , \tag{8}$$

where sing stands for single crystal, N is the number of lattice sites per unit volume in the host, and C is the fractional impurity concentration. In particular, the magnetization along the symmetry axis (c axis) of a single crystal is obtained from Eq. (8) by setting $\theta=0,\phi=0$, while the magnetization in the plane perpendicular to the symmetry axis is obtained by setting $\theta=\pi/2,\phi=0$.

For a polycrystalline sample, an additional average must be performed over all the possible orientations of the individual crystallites or, in other words, over all possible orientations of the c axis in Fig. 1. This average is calculated *after* the average over the internal field within a single crystallite has been completed. Thus the polycrystal magnetization becomes

$$M_{\rm poly}=\frac{1}{2\pi}\int_0^{2\pi}\int_0^{\pi/2}M_{\rm sing}(\theta,\phi)\sin\theta\,d\theta\,d\phi\ , \tag{9}$$

where poly stands for polycrystal.

III. NUMERICAL METHODS

The integrals appearing in expressions (8) and (9) for the magnetization cannot be performed analytically and require the application of numerical techniques. All the integrals were evaluated using the Gauss-Legendre quadrature in the form[18]

$$\int_a^b f(x)dx\cong\frac{b-a}{2}\sum_{i=1}^{n}w_i f\frac{(b-a)y_i+b+a}{2}\ , \tag{10}$$

where the y_i are the roots of the Legendre polynomial $P_n(y)$ of degree n and the weight factors w_i are given by

$$w_i=\frac{1}{(1-y_i^2)[P_n'(y_i)]^2}\ .$$

Values for y_i and w_i are tabulated by Stroud and Secrest.[18] A five-point scheme ($n=5$) was used

for all the angular integrations and a 40-point scheme ($n=40$) for the h integration. Moreover, since the form of the quadrature in Eq. (10) is appropriate for a finite interval from a to b, the upper limit of infinity on the h integral was replaced by a finite value $L(=130\Delta)$ in such a way that the internal field distribution $P(\vec{h})$ in Eq. (5) was normalized to 0.99. This procedure introduces a negligibly small error ($<0.05\%$) in the numerical results for the magnetization.

IV. APPLICATIONS

The expressions for the magnetization derived in Sec. II were applied to two different systems: single-crystal *Mg*Mn and polycrystalline *Zn*Mn. Both systems have been analyzed previously[2-4] using a spin Hamiltonian similar to that in Eq. (1) but containing only the crystal-field and external field terms (no RKKY term). For the *Mg*Mn system, this analysis yielded an effective spin for the Mn impurity of $S=\frac{5}{2}$ (assuming $g=2$) and a fine-structure splitting parameter of $D=+0.006K$, while for the *Zn*Mn system the values obtained for the effective impurity spin and the fine-structure parameter were $S=1$ and $D=-0.070K$, respectively. These results are used in the following discussion.

A. Single-crystal MgMn

Figure 2 shows the magnetization per ppm of impurity along the c axis of a 5 ppm single crystal of *Mg*Mn, plotted as a function of $1/T$. The solid curves represent the calculated c axis magnetization using the model described above while the error bars on the data points correspond to an estimated error of $\pm 15\%$ in the analyzed Mn concentration. For the c axis magnetization, the appropriate Hamiltonian is obtained by setting $\theta=0$ and $\phi=0$ in Eq. (3), so that the direction of the external field H_0 coincides with that of the symmetry axis (c axis) in Fig. 1:

$$\mathcal{H}_c = g\mu_B H_0 S_z + g\mu_B H\,(S_x\sin\theta'\cos\phi' + S_y\sin\theta'\sin\phi' + S_z\cos\theta') + D[S_z^2 - \tfrac{1}{3}S(S+1)]\,. \tag{11}$$

The solid curves in Fig. 2 were obtained by computing the matrix elements of the Hamiltonian,

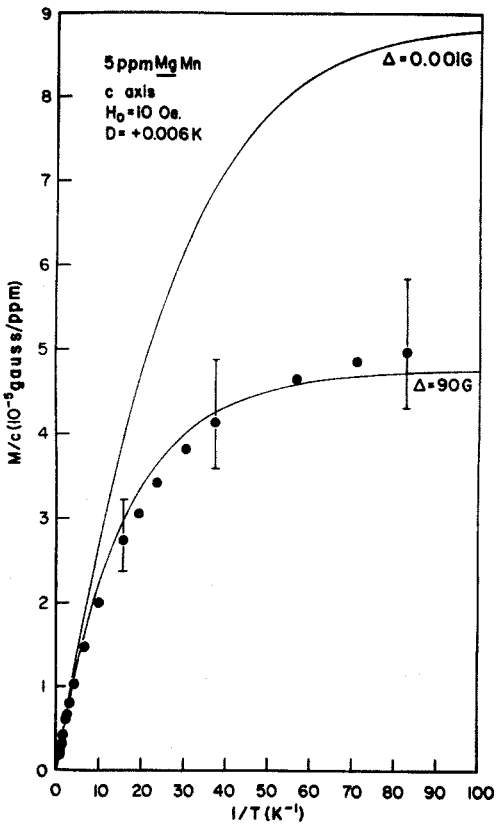

FIG. 2. Magnetization along the c axis of a 5 ppm single crystal of *Mg*Mn as a function of the reciprocal temperature.

$\langle M_s' \mid \mathcal{H}_c \mid M_s \rangle$ where the $\mid M_s \rangle$ are the eigenstates of S_z, diagonalizing the associated 6×6 matrix for $S=\frac{5}{2}$ and $D=+0.006K$ to obtain the eigenvalues and eigenvectors, and then using Eqs. (7) and (8) to calculate the magnetic moment per impurity ($\bar{\mu}$) and the magnetization. The curve for $\Delta=0.001$ G illustrates the effect of the crystal field in the presence of a negligibly small internal RKKY field [since the upper limit on the h integral in Eq. (8) was replaced by a value proportional to Δ, setting $\Delta=0$ causes the h integral, and hence the magnetization, to vanish], while the curve for $\Delta=90$ G provides the best fit to the experimental data. Similar fits to the data points corresponding to the extreme ends of the error bars in Fig. 2 yield lower and upper bounds for Δ of 56 and 125 G, respectively.

Figure 3 shows the probability distribution for the modulus of the internal field, $P(h)=4\pi h^2 P(\vec{h}) = 4\Delta h^2/\pi(\Delta^2+h^2)^2$, the thermal average of the magnetic moment per impurity $\bar{\mu}$ (in units of $g\mu_B$), and the product $\bar{\mu}P(h)/g\mu_B$, which appears in the integrand of Eq. (8), plotted as a function of the

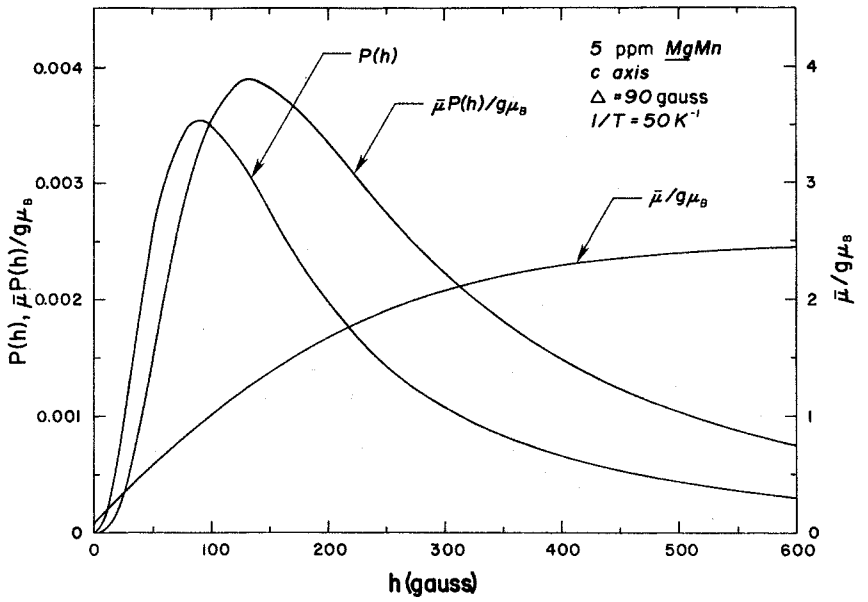

FIG. 3. Probability distribution for the modulus of the internal field $P(h)$, the thermal average of the magnetic moment per impurity $\bar{\mu}$, and the product $\bar{\mu}P(h)/g\mu_B$ as a function of internal field h at $1/T=50$.

internal RKKY field h for the special case where $\theta'=0$ and $\phi'=0$, and for $\Delta=90$ G and a fixed inverse temperature of $1/T=50$ K^{-1}. The probability distribution $P(h)$ possesses a "hole" at the origin ($h=0$) and a sharp peak at the most probable internal field Δ, while the impurity moment $\bar{\mu}$ increases monotonically with internal field and eventually saturates above $h\sim1000$ G. It should be pointed out that, in the present calculation, the most probable internal field Δ, and hence the probability distribution $P(h)$, is assumed to be independent of temperature. Since random molecular-field theories of spin-glasses require Δ to vanish above the spin-glass freezing temperature,[19,20] the present form of the model does not yield an abrupt transition between the spin-glass and paramagnetic regimes, but instead relies on thermal energy to *gradually* render the RKKY fields ineffective as the temperature increases. However, a comparison of the calculated curves for $\Delta=90$ G and $\Delta=0.001$ G in Fig. 2 shows that, for sufficiently high temperatures, the calculated magnetization approaches single-impurity behavior in spite of the presence of a temperature-independent internal field distribution. (The tempetature dependence of Δ and its relationship to the spin-glass freezing temperature are currently being investigated in detail at the ppm level in the spin-glass system *Ag*Mn.)

Figure 4 shows the magnetization per ppm of impurity along the a axis of another 5 ppm single crystal of *Mg*Mn plotted as a function of $1/T$. For the a axis magnetization, the external field H_0 lies in the plane perpendicular to the symmetry axis (c axis) of the crystal, and the corresponding Hamiltonian is obtained by setting $\theta=\pi/2$ and $\phi=0$ in Eq. (3). As before, the eigenvalues and eigenvectors of $\mathscr{H}_a$ were determined by diagonalizing the 6×6 matrix representing the Hamiltonian for $S=\frac{5}{2}$, and Eqs. (7) and (8) were used to compute the magnetization. The solid curves in Fig. 4 correspond to the calculated a axis magnetization, with the curve for $\Delta=0.001$ G illustrates the effect of the crystal field for $D=+0.006K$ and for a vanishingly small internal field. The curve for $\Delta=56$ G provides the best fit to the measured a axis data, with similar fits to the extreme ends of the error bars in Fig. 4 yielding lower and upper bounds for Δ of 40 and 75 G, respectively. A comparison of the best-fit values for the most probable internal field along the a and c axis shows that Δ_a and Δ_c overlap within the experimental error, lending consistency to the assumption (implicit throughout the calculation) of an *isotropic* probability distribution $P(\vec{h})$.

B. Polycrystalline ZnMn

Figure 5 show the magnetization per ppm of impurity (in an external field $H_0=88.2$ Oe) of four

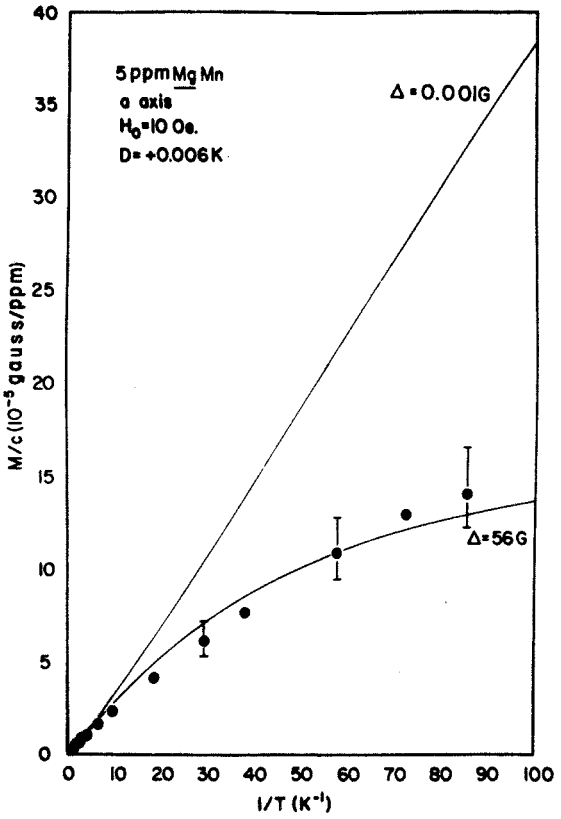

FIG. 4. Magnetization along the a axis of a 5 ppm single-crystal MgMn as a function of $1/T$.

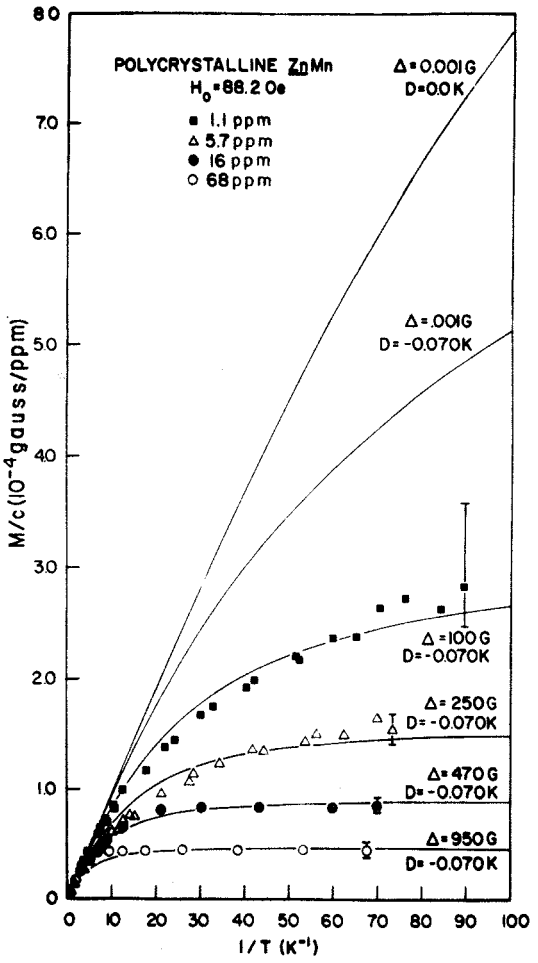

FIG. 5. Magnetization per ppm of impurity for polycrystalline ZnMn samples as a function of $1/T$.

polycrystalline samples of ZnMn with concentrations varying from 1.1 to 6.8 ppm Mn, plotted as a function of $1/T$. The solid curves in the figure represent the calculated magnetization for various values of the parameters D and Δ, while the error bars on the data points correspond to the following estimated uncertainties in the analyzed Mn concentrations: $C=1.1\pm0.2$, 5.7 ± 0.5, 16 ± 1, and 68 ± 7 ppm. For a polycrystalline system, the angles θ and ϕ, which specify the orientation of the c axis with respect to the external field (see Fig. 1), are now variables of integration and hence all the terms appearing in Eqs. (3), (4), and (6) must be included in the corresponding polycrystalline Hamiltonian. Moreover, since the Mn impurity has an effective spin of $S=1$ when dissolved in Zn, the eigenvalues and eigenvectors of the Hamiltonian are now obtained by diagonalizing a 3×3 matrix in the $|M_s\rangle$ representation, and the calculated magnetization is obtained from Eqs. (7)–(9) by averaging the single-crystal result for fixed θ and ϕ over all possible orientations of the crystallites.

The curve for $D=0K$ and $\Delta=0.001$ G in Fig. 5 shows the magnetization for a system of free impurity spins (i.e., a Brillouin function $S=1$) in the limit of zero crystal field and a negligible internal field, while the curve for $D=-0.070K$ and $\Delta=0.001$ G illustrates the effect of the crystal field appropriate to ZnMn (suitably averaged over all the crystallites) for a vanishingly small internal field. The remaining curves for $D=-0.070K$ and $\Delta=100$, 250, 470, and 950 G represent the best fits to the experimental data. Figure 6 shows a log-log plot of the best-fit values of Δ, the most probable internal field, for ZnMn as a function of the fractional impurity concentration C (in ppm). The vertical error bars in this figure were obtained by fitting the theoretical expression for the polycrystalline magnetization to the data points corresponding to the upper and lower ends of the error bars in Fig. 5. Random molecular-field theories of spin-glasses predict a variety of concentration

dependences for Δ: For the 3D Heisenberg model, with the internal field distribution $P(\vec{h})$ given by Eq. (5), Δ has been shown[13,15] to vary linearly with impurity concentration, while, for the 1D Ising model, Klein[19] has shown that the appropriate probability distribution has the form of a Lorentzian for small internal fields with $\Delta \propto C$, and a Gaussian for high internal fields with $\Delta \propto C^{1/2}$. For the *Zn*Mn system, the straight line in Fig. 6 corresponds to a concentration dependence of the form $\Delta = KC^n$ with $n = 0.56^{+0.07}_{-0.15}$ and $K = 94.8^{-20.4}_{+49.5}$ Gauss/(ppm)^n.

V. ESTIMATES FOR THE *s-d* COUPLING CONSTANT *J*

For a three-dimensional Heisenberg distribution of internal fields, the expression which relates the internal field parameter Δ (in ergs) and the impurity concentration C (in at. %) for an fcc lattice is given by[15,21]

$$\Delta = \left[\frac{Z^2 J^2 S}{2a^3 n E_F} \right] C , \tag{12}$$

where Z is the number of conduction electrons per atom, n is the density of conduction electrons, J is the *s-d* exchange constant (in ergs), E_F is the Fermi energy (in ergs), a is the lattice constant, and S is the impurity spin. In order to obtain the form appropriate to an hcp host, Eq. (12) is modified by replacing the site density for an fcc lattice $(4/a^3)$ by the corresponding site density for an hcp lattice $(4/\sqrt{3}ca^2)$:

$$\Delta = \left[\frac{Z^2 J^2 S 10^{-4}}{2\sqrt{3} g u_B c a^2 n E_F} \right] C , \tag{13}$$

where Δ is now in units of gauss and C is in units of ppm.

If the quantity in parentheses in Eq. (13) is assumed to be independent of the precise form of the concentration dependence for Δ, then equating this quantity with the value of K determined experimentally for the *Zn*Mn system in the preceding section, yields an estimate for the *s-d* exchange constant J. Taking $Z=2$, $n = 1.316 \times 10^{23}$ cm^{-3}, $E_F = 9.46$ eV, $c = 4.9469$ Å, and $a = 2.6647$ Å for Zn, and using $g=2$ and $S=1$ for the Mn impurity, we obtain

$$|J(Zn\text{Mn})| = 0.64^{+0.15}_{-0.07} \text{ eV} .$$

A similar estimate for the *Mg*Mn system was obtained by using Eq. (13), with C replaced by $C^{0.56}$, in conjunction with the experimentally determined values for Δ. Taking $Z=2$, $n = 8.261 \times 10^{22}$ cm^{-3}, $E_F = 7.313$ eV, $c = 5.2103$ Å, and $a = 3.2094$ Å for Mg, and using $g=2$ and $S = \frac{5}{2}$ for the Mn impurity (with $C = 5$ ppm) yielded for *Mg*Mn:

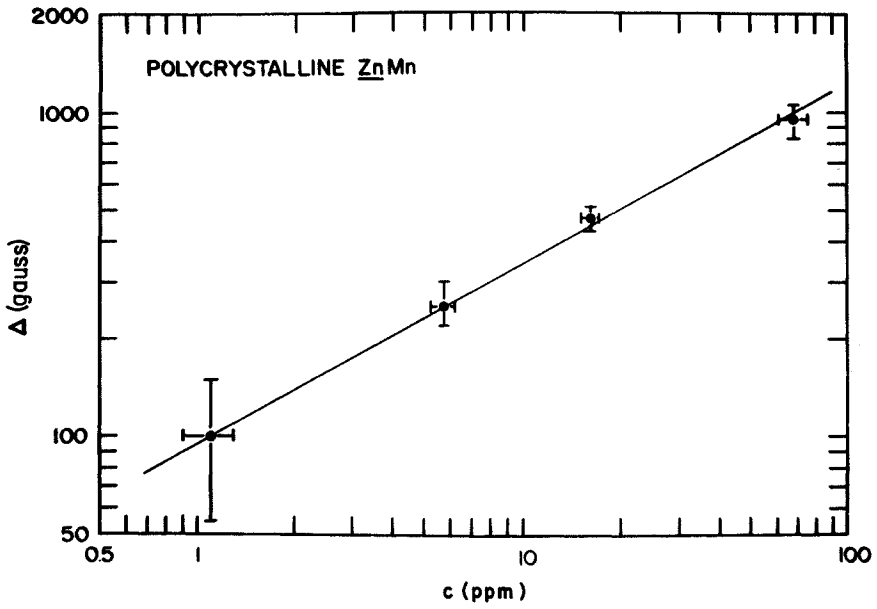

FIG. 6. Concentration dependence of the parameter Δ, the most probable value of the internal field, for polycrystalline *Zn*Mn.

$$|J(c \text{ axis})| = 0.22 \pm 0.04 \text{ eV} ,$$

$$|J(a \text{ axis})| = 0.18^{+0.02}_{-0.03} \text{ eV} ,$$

showing that the two values for J overlap within experimental error.

Our estimates for the s-d exchange parameter J are comparable to the values quoted in the literature for these and related systems. For ZnMn, Smith[22] obtained $|J| = 2.6$ eV, while Hedgecock and Rizzuto[23] obtained $|J| = 1.37$ eV. (Such variations in J may be a consequence of the different concentration regimes examined by the various authors, since a reduction in the mean free path of the conduction electrons leads to a self-damping of the RKKY interaction. We have neglected this effect in our analysis.) Our estimates for MgMn are also comparable to those obtained for MgGd ($J = 0.2$ eV) and MgEr ($J = 0.16$ eV) from the EPR measurements of Zimmermann *et al.*[24] It should be pointed out that the present analysis yields $|J(Mg\text{Mn})| < |J(Zn\text{Mn})|$; this is consistent with the fact that the effective spin of the Mn impurity in Mg ($S = 2.3$) is close to its free-ion value which implies less mixing between the impurity and the conduction electrons in the MgMn system.

IV. CONCLUSION

A simple physical model has been presented for dilute magnetic systems with hcp hosts which is capable of accounting for both single-impurity effects as well as impurity-impurity interaction effects. Numerical calculations of the magnetization as a function of temperature, based on the model, have been compared with the measured magnetization for two representative systems, MgMn and ZnMn, and estimates were obtained for both the internal field parameter Δ and the s-d exchange constant J. The analysis also showed that, for the ZnMn system, Δ varies with impurity concentration as $C^{0.56}$. The model also serves to illustrate an important point: Owing to the long-ranged nature of the RKKY coupling, impurity-impurity interaction effects are significant even for impurity concentrations of the order of 1 ppm and can lead to substantial modifications in the single-impurity behavior, at least over the temperature range of the present investigation (10 mK $\leq T \leq$ 2 K). Moreover, it seems remarkable that a model which relies so heavily on ionic concepts, even in the presence of a large conduction-electron–local-electron mixing interaction, provides such an excellent description of the experimental data in dilute *metallic* systems.

ACKNOWLEDGMENTS

This research was supported by the National Science Foundation under Grant No. DMR-7916243. One of us (R.R.) would like to thank the National Research Council of Canada for a Fellowship.

*Present address: Natural Science Division, Shasta Community College, Redding, California.

[1]J. C. Doran, S. F. Kral, T. Steelhammer, and O. G. Symko, Solid State Commun. 17, 1099 (1975).
[2]S. F. Kral, L. A. Moberly, T. Steelhammer, and O. G. Symko, Solid State Commun. 32, 671 (1979).
[3]L. Moberly, R. Roshko, and O. G. Symko, Bull. Am. Phys. Soc. 25, 306 (1980).
[4]L. Moberly, R. Roshko, and O. G. Symko (unpublished).
[5]L. L. Hirst, Z. Phys. 241, 9 (1971).
[6]A. Blandin and J. Friedel, J. Phys. Radium 19, 573 (1958).
[7]P. W. Anderson, Phys. Rev. 124, 41 (1961).
[8]A. Abragam and B. Bleaney, *Electron Paramagnetic Resonance of Transition Ions* (Clarendon, Oxford, 1970), p.157.
[9]P. S. Riseborough, Phys. Rev. B 20, 1362 (1979).
[10]B. Caroli, J. Phys. Chem. Solids 28, 1427 (1967).
[11]M. A. Ruderman and C. Kittel, Phys. Rev. 96, 99 (1954); T. Kasuya, Prog. Theor. Phys. 16, 45 (1956); K. Yosida, Phys. Rev. 106, 893 (1957).
[12]M. W. Klein, Phys. Rev. 188, 933 (1969); M. W. Klein and R. Brout, *ibid.* 132, 2412 (1963).
[13]N. Rivier and K. Adkins, in *Amorphous Magnetism*, edited by H. O. Hooper and A. M. de Graaf (Plenum, New York, 1973), pp. 215–225.
[14]C. Held, and M. K. Klein, Phys. Rev. Lett. 35, 1783 (1975).
[15]L. R. Walker and R. E. Walstedt, Phys. Rev. B 22, 3816 (1980).
[16]A. H. Morrish, *The Physical Principles of Magnetism* (Wiley, New York, 1965), pp. 119–123.
[17]C. P. Poole and H. A. Farach, *The Theory of Magnetic Resonance* (Wiley, New York, 1972).
[18]A. H. Stroud and D. Secrest, *Gaussian Quadrature*

Formulas (Prentice-Hall, Englewood Cliffs, 1966).
[19]M. W. Klein, Phys. Rev. B 14, 5008 (1976).
[20]I. Reiss and M. W. Klein, Phys. Rev. B 15, 6001 (1977).
[21]F. W. Smith, Phys. Rev. B 14, 241 (1976).
[22]F. W. Smith, Phys. Rev. B 10, 2980 (1974).
[23]F. T. Hedgecock and C. Rizzuto, Phys. Rev. 103, 517 (1967).
[24]P. H. Zimmermann, D. Davidov, R. Orbach, L. J. Tao, and J. Zitkova, Phys. Rev. B 6, 2783 (1972).